Earthquake Geotechnical Engineering for Protection and Development of Environment and Constructions – Silvestri & Moraci (Eds)
© 2019 Associazione Geotecnica Italiana, Rome, Italy, ISBN 978-0-367-14328-2

Co-seismic rotation and displacement of a structure with a basement sited in liquefiable soil

F.E. Hughes & S.P.G. Madabhushi
Department of Engineering, University of Cambridge, UK

ABSTRACT: The inclusion of basements can provide uplift forces during earthquake induced liquefaction thereby reducing the overall settlement of structures. When the vertical forces acting on the structure are not co-linear, due to building geometry, inter-storey drift, rocking or rotation of the structure, this uplift force increases the moment acting on the structure. A series of dynamic geotechnical centrifuge tests has been conducted to investigate the co-seismic behaviour of structures with basements sited in liquefiable soil. Particle image velocimetry (PIV) was undertaken using GeoPIV-RG to obtain co-seismic displacements. In this paper, the stability of such structures during the liquefied period will be investigated, and compared to the behaviour of structures on shallow foundations without basements. It will be shown that a structure with a basement can suffer severe rotations in strong earthquake events, although the overall settlements are reduced.

1 INTRODUCTION

Earthquake induced liquefaction is continuing to cause significant damage in the built environment. On level ground, this is primarily due to its effect on structures with shallow foundations, which have been repeatedly observed to experience rotation and large settlement (Cubrinovski et al. 2011; Yasuda et al. 2012; Bertalot et al. 2013). Significant research has been conducted to investigate the effect of a number of parameters on this failure type, including the depth of the liquefiable layer, structure bearing pressure, width of the structure and shaking intensity to name a few (Dashti et al. 2010; Bertalot & Brennan 2015; Adamidis & Madabhushi 2018). Another highly researched problem caused by liquefaction in the built environment is the uplift of subsurface structures which have a unit weight lower than the liquefied soil surrounding them - for example pipe lines, empty storage tanks or underground car parks (Koseki et al. 1997; Yang et al. 2004; Chian & Madabhushi 2012).

The behaviour of structures partially buried in liquefiable ground, which is the case for many modern buildings with basements, is not well understood. Intuitively, buildings of this nature combine the propensity of surface structures to settle and light subsurface structures to float, and therefore may result in a reduced total vertical displacement. Wide basements have been found to successfully reduce settlement, rotation and seismic demand of a structure if the ratio of the vertical forces and the eccentricity of the centre of mass are controlled (Hughes & Madabhushi 2019). This aim of this paper is to look at whether this is possible for a structure with a narrow basement.

2 EXPERIMENTAL METHODS

A series of dynamic centrifuge experiments has been undertaken at the University of Cambridge, using the 10 m diameter beam centrifuge at the Schofield Centre (Schofield 1980). Results from two of these centrifuge tests will be presented in this paper.

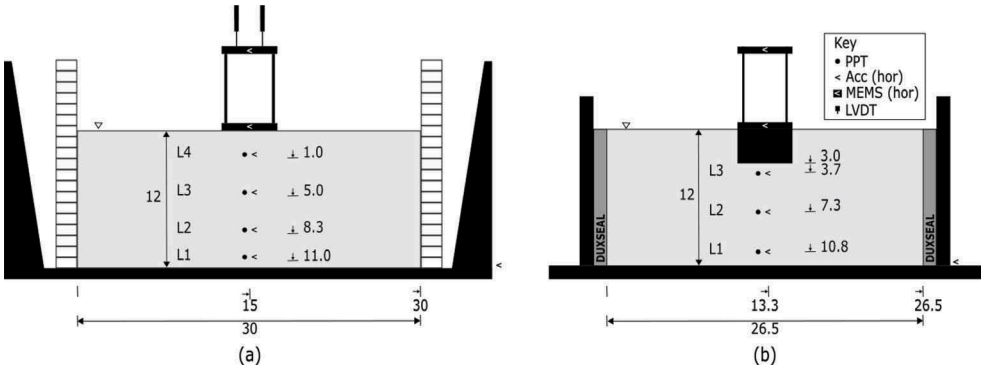

Figure 1. Centrifuge model layout and location of instruments discussed in this paper. (a) Structure on shallow foundation in a laminar container. (b) Structure with a basement in a rigid container with a Perspex window. Dimensions in metres, prototype scale.

The first test discussed in this paper investigated the behaviour of a structure on a shallow foundation with no basement (Figure 1a). It was conducted in a laminar container (Brennan et al. 2006), the model container best suited to liquefaction problems. The second test discussed in this paper investigated the behaviour of a structure with a basement and was conducted in a rigid container with a Perspex window which allowed digital image correlation to be conducted (Figure 1b). A layer of Duxseal at both ends of the container was used to limit the effect of the rigid boundaries (Steedman & Madabhushi 1991). It is recognised that absorbing boundaries such as Duxseal layers are only partially effective especially when soil stiffness degrades significantly during liquefaction events. The advantage of being able to conduct digital image correlation was believed to outweigh the trade off regarding the boundary conditions.

A liquefiable layer of loose Hostun HN31 sand with a target relative density of 44 % was prepared by air pluviation using an automatic sand pourer (Chian et al. 2010). Properties of the Hostun sand used are as follows: G_s = 2.65, d_{50} = 0.424 mm, e_{min} = 0.555, e_{max} = 1.01 and φ_{crit} = 33° (Mitrani 2006). Arrays of instruments were placed on and underneath each structure. Piezoelectric accelerometers (Acc), linear variable differential transformers (LVDTs), micro mechanical system accelerometers (MEMS) and pore pressure transducers (PPTs) were used. The locations of the instruments discussed in this paper are shown in Figure 1.

The model structures used consisted of a single degree of freedom (SDOF) sway frame. For the test with a basement, this superstructure was rigidly connected to a rigid basement structure which was constructed out of sheet aluminium surrounding closed-cell foam. The basement was the same width as the superstructure. The derivation of the buoyancy force acting on a structure with a basement when full liquefaction occurs ($F_{U,L}$) is described in detail by Hughes & Madabhushi 2019, and the result is given in Equation 1 below:

$$F_{U \cdot L} = \gamma_s V \tag{1}$$

where γ_s is the saturated unit weight of the soil and V is the volume of the basement submerged. Structure properties, in prototype scale, are given in Table 1. Total and effective bearing pressures are respectively the total and effective vertical stress applied by the combined superstructure and basement (where applicable) to the soil directly beneath the structure.

The tests were conducted at a centrifugal acceleration of 60 g. The models were saturated with a high viscosity aqueous solution of hydroxypropyl methylcellulose with a viscosity of 60 cSt. This was done using CAM-Sat, an automated, pressure controlled system (Stringer & Madabhushi 2010). A stored-angular momentum (SAM) actuator was used to generate sinusoidal input motions (Madabhushi et al. 1998). The characteristics of the base shaking events

Table 1. Properties of structures (prototype scale)

Property	No Basement	With Basement
Total bearing pressure (static) (kPa)	44.3	65.3
Effective bearing pressure (static) (kPa)	44.3	38.5
Superstructure width (m)	4.8	4.8
Basement width (m)	NA	4.8
Basement depth (m)	NA	3.0
Fixed base natural frequency (Hz)	1	1

Table 2. Characteristics of base shaking (prototype scale)

Property	No Basement	With Basement
Peak acceleration (g)	0.21	0.16
No of cycles	20	20
Frequency (Hz)	1	1
Input/struct fixed base natural frequency	1	1
Arias intensity (m/s)	2.0	1.3
Significant duration (s)	13.8	13.7

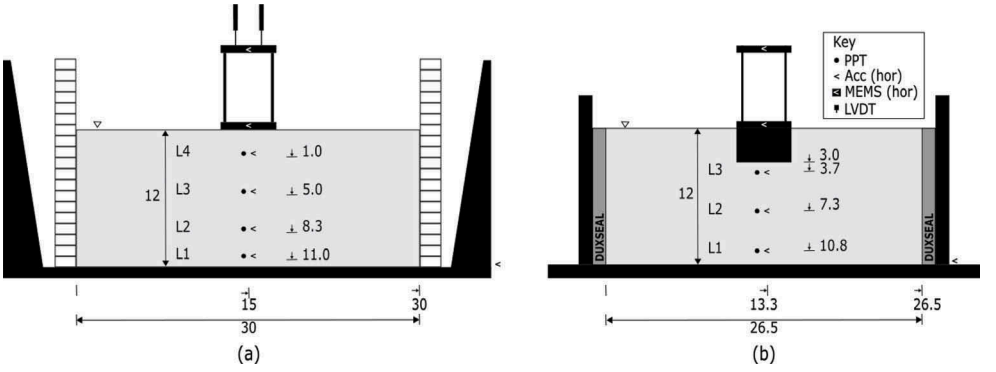

Figure 2. Excess pore pressure ratio, $r_u(t)$, in the column of soil beneath the centre of the structure, and the input motion. Left column: structure without a basement. Right column: structure with a basement.

discussed in this paper are given in Table 2. In this table the last row shows the duration of significant shaking, which corresponds to the time between dissipation of 5 % and 95 % of the total Arias intensity (Arias 1970). Higher harmonics in the base shaking were more significant in the test conducted in the laminar container compared to the rigid container (Figure 2).

For the test conducted in the rigid container with a Perspex window, particle image velocimetry (PIV) analysis was conducted using GeoPIV-RG to obtain displacements of the soil and structure (White et al. 2003; Stanier et al. 2015). A MotionBLITZ EoSens mini2 high-speed recording camera was used to record the cross section visible through the Perspex window. Images were captured at a frame rate of 804 Hz using an exposure time of 100 μs. The image size was 1696 1116 pixels.

3 SOIL RESPONSE

Excess pore pressure ratio, $r_u(t)$, is defined in Equation 2 and is plotted in Figure 2 for the instrumented locations beneath the centre of each of the structures tested.

$$r_u(t) = u_{ex}(t)/\sigma'_{v0} \quad (1)$$

where $u_{ex}(t)$ is the excess pore pressure generated and σ'_{v0} is the initial vertical effective stress at the corresponding location. The initial vertical stress was calculated by adding the bearing pressure applied by the structure to the stress caused by the soil between the bottom of the structure and the instrument. The onset of base shaking caused excess pore pressures to be generated at all instrumented depths beneath each of the structures tested (Figure 2). A reduction in effective vertical stress ensued which resulted in a very large stiffness degradation of the sand. Transmission of horizontal shear waves therefore decreased, causing horizontal accelerations to be attenuated as they were transmitted upwards from the base of the model (Figure 3).

Under the structure without a basement, the greatest excess pore pressure ratio was recorded at the deepest instrumented depth. The excess pore pressure ratio rapidly increased to a maximum value of approximately 0.5 at the three deepest instrumented depths (L1-3) and increased at a slower rate to a maximum of only 0.3 at the shallowest depth (L4). A bulb of non-liquefiable soil formed beneath the structure, below which sufficient soil softening occurred to isolate the structure from the base shaking. This is in agreement with the observations of Adamidis & Madabhushi 2018 for a structure with a comparable bearing pressure resting on a deep liquefiable layer. The accelerations transmitted to the ground floor of the structure were therefore smaller than the base shaking (Figure 3).

In comparison, under the structure with a basement the greatest excess pore pressure ratios were recorded at the shallowest instrumented depth beneath the structure (L3). Full liquefaction occurred at this depth, isolating the structure from the base shaking. When full liquefaction occurred, the effective bearing pressure applied by this structure decreased to approximately

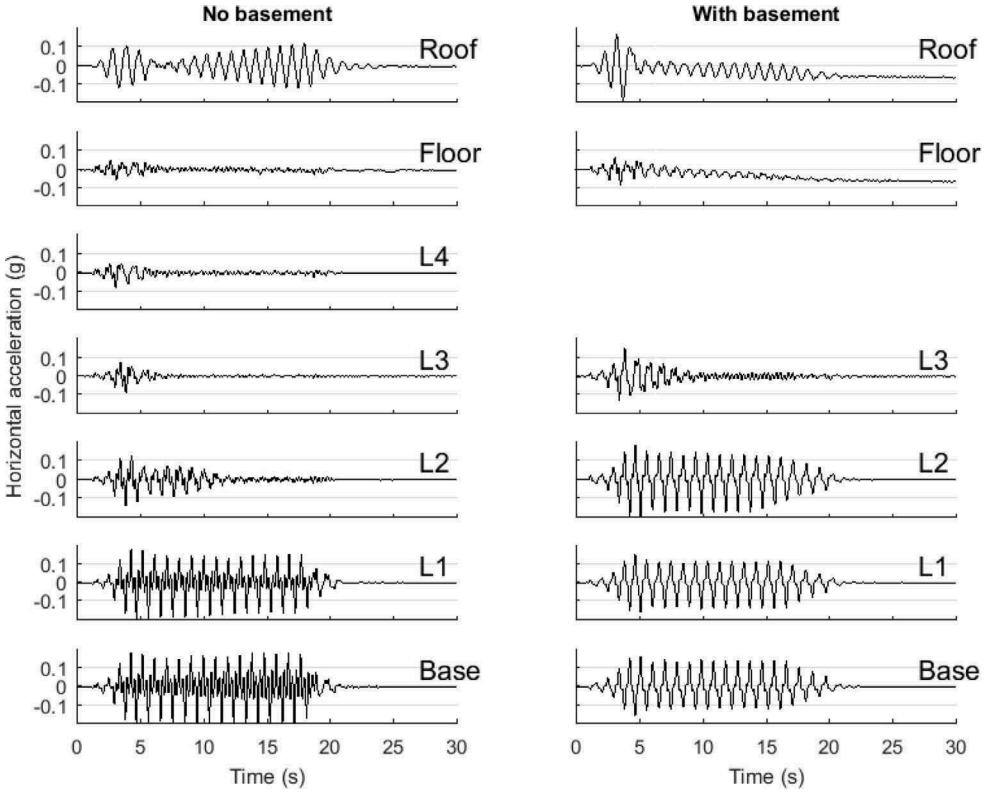

Figure 3. Co-seismic horizontal accelerations of the structures, the instrumented locations in the column of soil beneath the centre of the structures, and the input motion. Left column: structure without a basement. Right column: structure with a basement.

11.2 kPa, as the buoyancy force provided by the basement increased. Once significant excess pore pressures had been generated, the accelerations at roof level were less than the base shaking, with the amplification ratio remaining approximately 0.3 for the remainder of shaking (Figure 3). Accumulated rotation of the structure, which is discussed in detail in Section 4, caused the observed drift in the measured horizontal acceleration of the structure roof and floor. As the accumulated rotation of the structure increased, the MEMS recorded an increasing component of the centrifugal acceleration.

4 DISPLACEMENT AND ROTATION OF STRUCTURES

The vertical displacement and rotation of a structure with and without a basement are compared in Figure 4, and were obtained using geoPIV-RG and LVDTs respectively.

The structure with no basement settled 0.43 m, prototype scale. Most of this was accumulated during the co-seismic period, with a small amount occurring post-shaking. This is a comparable magnitude to other dynamic centrifuge investigations looking at structures with shallow foundations, without a basement, sited on deep layers of liquefiable soil (Bertalot & Brennan 2015; Adamidis & Madabhushi 2018). The structure experienced minimal rotation, totalling less than 0.5 degrees.

The presence of a basement had the positive desired effect of notably reducing the settlement of the structure, to 0.15 m (Figure 4). However, significant rotation was accumulated. Anitclockwise rotation was accumulated at an approximately constant rate during shaking, totalling 4.0 degrees at the end of shaking. Rotation and settlement of the structure stopped when shaking ceased.

5 SOIL DEFORMATIONS

Soil displacements were obtained for the structure with a basement using using GeoPIV-RG (White et al. 2003; Stanier et al. 2015). Total co-seismic soil displacement contours are shown in Figure 5. The soil displacements shown are relative to the movement of the rigid model container, and are plotted at the initial location of each tracked patch. The position of the basement at the end of shaking is shown.

As expected, asymmetry in the soil displacements was observed. This is in contrast to the almost symmetric accumulated vertical and horizontal displacements observed for structures on shallow foundations on liquefied layers of varying depths by Adamidis & Madabhushi 2018. For a structure with a narrow basement presented here, the greatest soil displacements occurred to the left of the structure and below the bottom left of the structure, as the structure moved into this space. Below the bottom of the basement, at a distance of B/3 from the left hand corner of the basement, soil displaced vertically downwards, with no horizontal component. To the left and right of this, vertical displacement was accompanied by horizontal displacement, to the left and right respectively. No gap was formed underneath the structure. Instead, the liquefied soil moved with the rotating basement. Sand accumulated below the basement, resulting in accumulation of permanent rotation.

6 MOMENTS TRANSMITTED FROM STRUCTURE TO UNDERLYING SOIL

The moments transmitted from the structure to the underlying soil consist of three components. The first component is the P - δ effect due to the vertical forces not being co-linear. This is increased by inter-storey drift, rocking or rotation of the structure. The second component is provided by the inertial force of the masses accelerating due to the transmission of the base shaking through the soil body to the structure. This is reduced when the structure is isolated due to liquefaction of the soil beneath the structure. The third contribution comes from the rotational inertia of the components of the structure. Net moments transmitted from the

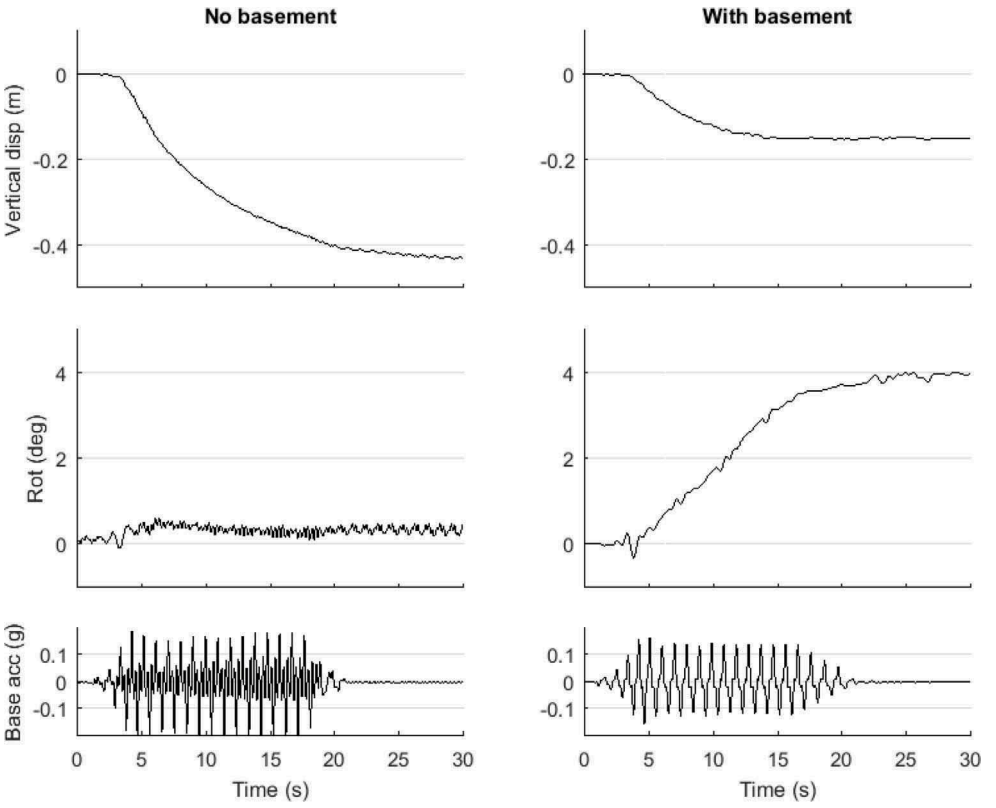

Figure 4. Vertical displacement and rotation, prototype scale. Left column: structure without a basement. Right column: structure with a basement. Settlement is negative vertical displacement and anticlockwise rotation is positive.

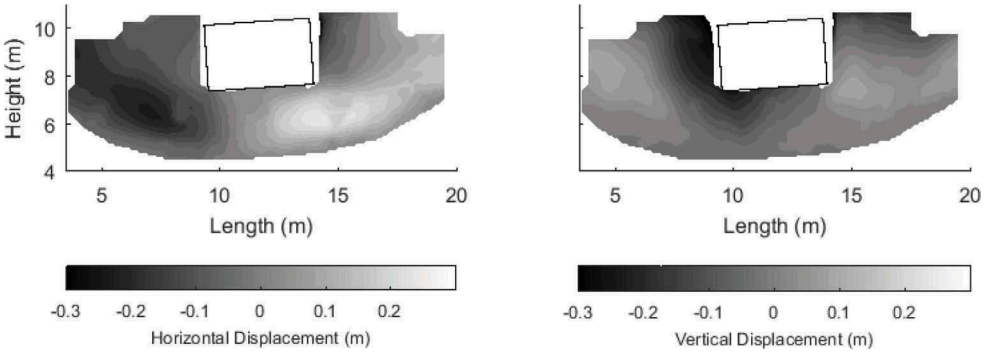

Figure 5. Total soil displacement for structure with basement, prototype scale.

structure to the underlying soil were calculated about the right hand corner of the bottom of the basement, which was identified as the point of rotation from the high speed images taken, and are shown in Figure 6. Anticlockwise moments and rotations are taken as positive.

The peak moment transmitted from the structure to the surrounding soil occurred during the first cycle of shaking, before the soil fully liquefied (Figure 3). Once liquefaction had occurred, the dynamic component of the moments reduced as the structure was isolated and the accelerations transmitted to the structure reduced. However, the static component of the moment

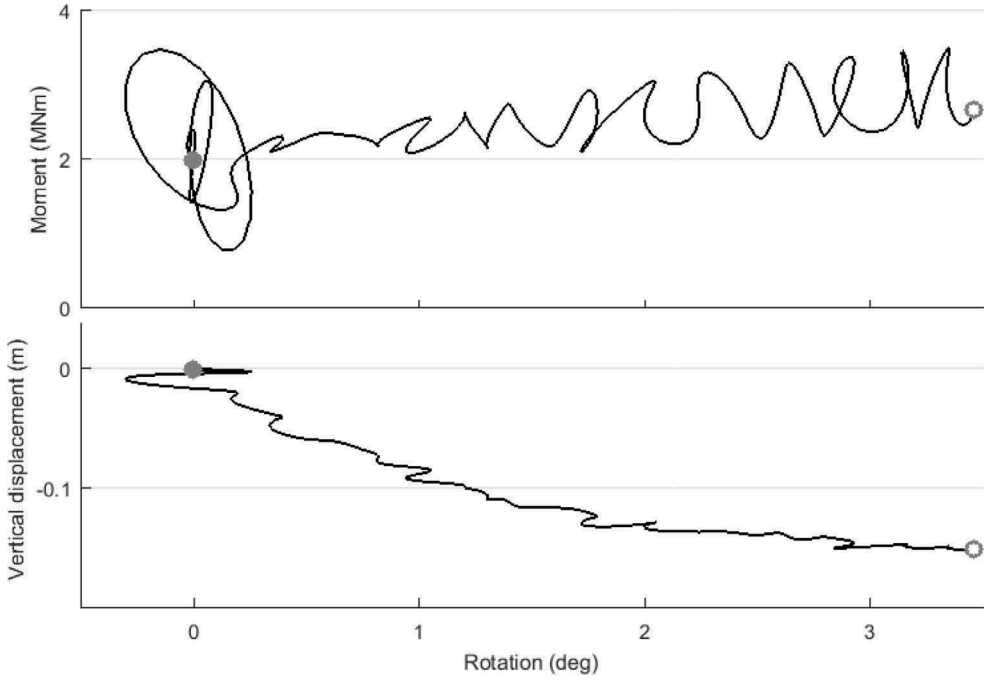

Figure 6. Co-seismic moment-rotation and rotation-vertical displacement behaviour of a structure with a basement. Moments taken about the right hand corner of the bottom of the basement. Anticlockwise moments and rotations are positive. Settlement is negative vertical displacement. Start of base shaking located by filled grey circle and end of base shaking by open grey circle.

increased, as anticlockwise rotation was accumulated and the moment due to the P – δ effect increased. This moment further increased the rotation of the structure, rather than re-righting the structure which is the case for stable ships. Insufficient resistance was provided by the shear dilation of the liquefied soil adjacent to the basement to prevent the structure rotating.

7 CONCLUSIONS

In this paper, the co-seismic behaviour of a structure with a narrow basement sited in liquefiable soil has been discussed in detail, and has been compared to the behaviour of a structure on a shallow foundation. The presence of the basement had the desirable effect of notably reducing the settlement of the structure. The buoyancy force provided by the basement prevented the structure with a basement settling as much as a structure without a basement. Liquefaction caused both structures to be isolated from base shaking, reducing the seismic demand of the structures. A bulb of non-liquefied soil formed beneath the structure without a basement. Significant soil softening occurred beneath that bulb, which isolated the structure. In contrast, isolation of the structure with a basement occurred due to full liquefaction directly beneath the basement. This is in contrast to other remediation methods used to reduce liquefaction induced settlement of structures, which have the adverse affect of increasing the accelerations transmitted to the structures (Mitrani 2006; Zeybek & Madabhushi 2016; Olarte et al. 2018).

However, the presence of a basement caused the structure to experience greater rotation than structures without basements. The structure rotated anticlockwise about the right hand corner of the narrow basement, and accumulated rotation at an approximately constant rate after liquefaction occurred. The moment due to the P - δ effect increased as the structure accumulated rotation and further increased the rotation of the structure, rather than re-righting

the structure. Insufficient resistance was provided by the shear dilation of the liquefied soil adjacent to the structure to prevent the structure rotating.

REFERENCES

Adamidis, O. & Madabhushi, S.P.G., 2018. Deformation mechanisms under shallow foundations on liquefiable layers of varying thickness. Géotechnique, 68(7), pp.602–613.

Arias, A., 1970. A measure of earthquake intensity R. J. Hansen, ed., Cambridge, Massachusetts: MIT Press.

Bertalot, D. & Brennan, A.J., 2015. Influence of initial stress distribution on liquefaction-induced settlement of shallow foundations. Géotechnique, 65(5), pp.418–428.

Bertalot, D., Brennan, A.J. & Villalobos, F.A., 2013. Influence of bearing pressure on liquefaction-induced settlement of shallow foundations. Géotechnique, 63(5), pp.391–399.

Brennan, A.J., Madabhushi, S.P.G. & Houghton, N.E., 2006. Comparing laminar and equivalent shear beam (ESB) containers for dynamic centrifuge modelling. In 6th International Conference on Physical Modelling in Geotechnics. Hong Kong, pp. 171–176.

Chian, S.C. & Madabhushi, S.P.G., 2012. Effect of buried depth and diameter on uplift of underground structures in liquefied soils. Soil Dynamics and Earthquake Engineering, 41(1), pp.181–190.

Chian, S.C., Stringer, M.E. & Madabhushi, S.P.G., 2010. Use of automatic sand pourers for loose sand models. In 7th International Conference on Physical Modelling in Geotechnics. Zurich, Switzerland, pp. 117–121.

Cubrinovski, M. et al., 2011. Soil Liquefaction Effects in the Central Business District during the February 2011 Christchurch Earthquake. Seismological Research Letters, 82(6), pp.893–904.

Dashti, S. et al., 2010. Centrifuge Testing to Evaluate and Mitigate Liquefaction-Induced Building Settlement Mechanisms. Journal of Geotechnical and Geoenvironmental Engineering, 136(7), pp.918–929.

Hughes, F.E. & Madabhushi, S.P.G., 2019. Liquefaction Induced Displacement and Rotation of Structures with Wide Basements. Soil Dynamics and Earthquake Engineering, 120, pp.75–84.

Koseki, J., Matsuo, O. & Koga, Y., 1997. Uplift behaviour of underground structures caused by liquefaction of surrounding soil during earthquake. Soils and Foundations, 37(1), pp.97–108.

Madabhushi, S.P.G., Schofield, A.N. & Lesley, S., 1998. A new stored angular momentum (SAM) based earthquake actuator. In Proceedings of the International Conference Centrifuge 98. pp. 111–116.

Mitrani, H., 2006. Liquefaction Remediation Techniques for Existing Buildings. University of Cambridge.

Olarte, J.C. et al., 2018. Effects of drainage control on densification as a liquefaction mitigation technique. Soil Dynamics and Earthquake Engineering, 110, pp.212–231.

Schofield, A.N., 1980. Cambridge Geotechnical Centrifuge Operations. Géotechnique, 30(3), pp.227–268.

Stanier, S.A. et al., 2015. Improved image-based deformation measurement for geotechnical applications. Canadian Geotechnical Journal, 53(5), pp.727–739.

Steedman, R.S. & Madabhushi, S.P.G., 1991. Wave propagation in sand medium. In Proceedings of the 4th International Conference on Seismic Zonation. Stanford, California.

Stringer, M.E. & Madabhushi, S.P.G., 2010. Improving model quality through computer controlled saturation. In 7th International Conference on Physical Modelling in Geotechnics. Zurich, Switzerland, pp. 171–176.

White, D.J., Take, W.A. & Bolton, M.D., 2003. Soil deformation measurement using particle image velocimetry (PIV) and photogrammetry. Géotechnique, 53(7), pp.619–631.

Yang, D. et al., 2004. Numerical Model Verification and Calibration of George Massey Tunnel using Centrifuge Models. Canadian Geotechnical Journal, 41(5), pp.921–942.

Yasuda, S. et al., 2012. Characteristics of liquefaction in Tokyo Bay area by the 2011 Great East Japan Earthquake. Soils and Foundations, 52(5), pp.793–810.

Zeybek, A. & Madabhushi, S.P.G., 2016. Centrifuge testing to evaluate the liquefaction response of air-injected partially saturated soils beneath shallow foundations. Bulletin of Earthquake Engineering, 15 (1), pp.339–356.